Transactions of the Korean Nuclear Society Fall Meeting
Yeosu, Korea, October 24-26, 2018

Oxidation behavior of Ni-Cr-Fe alloys with different Cr content in simulated PWR primary water

Hee-Sang Shim*, Do Haeng Hur

Nuclear Materials Research Division, KAERI, 989-111 Daedeok-daero, Yuseong-gu, Daejeon 34057, Korea
**Corresponding author: hshim@kaeri.re.kr*

1. Introduction

The reduction of occupational radiation exposure is one of the important issues in the water chemistry of nuclear power plants. In a pressurized water reactor (PWR), Co-58 and Co-60 are known as the major sources of the radiation field and produced by a radioactivation of Ni-58 and Co-59, respectively. Ni is released from the surface of various Ni-base structural materials such as steam generator tubes and CRDM nozzles because these not only consist of 58-72% nickel but also occupy over 70% of the total surface area exposed to the coolant [1]. Therefore, it is apparent that mitigation of Ni release from the Ni-base alloys should be a crucial strategy for source term reduction in PWRs. Since the steam generator tubing material has been replaced from Alloy 600 to Alloy 690, the Co-58 radiation filed has been reported to be significantly reduced. This is because the resistance of Ni release is improved in the corrosion environment of PWR primary coolant due to the increase of Cr content.

The diffusion of metal elements into the coolant through the passive layer is depressed due to the increase of the Cr content because increasing Cr content in Ni-base alloys enhances the protectiveness of passive film [2,3]. Actually, the passive film, Cr_2O_3, was reported to be stably formed when the Cr content in Ni-base alloys is larger than about 17wt%, although the critical concentration of Cr for passive film formation depends on many environmental factors such as hydrogen concentration, water chemistry and coolant flow rate. Based on such a background, Alloy 600 (Ni-16Cr-9Fe) and Alloy 690 (Ni-30Cr-9Fe) have been employed as a significant structural material in PWRs. In addition, the corrosion characteristics of these materials have been widely studied in various environmental conditions [4]. However, many works have been interested on stress corrosion cracking (SCC) or environmental corrosion researches [5,6], and studies on corrosion release in terms of source reduction have rarely been done. In general, the release rate of metals has been known to be proportional to their general corrosion rate and depends on a kinds of materials [7].

In this work, the corrosion rate and oxidation behaviors of the Ni-Cr-Fe alloys with increasing a Cr content were investigated in simulated primary water at 330ºC. The structural and electrochemical properties of the alloys were analyzed by using XRD, SEM and potentiostat analyzer. The properties of the oxidation films were investigated by using SEM, XRD, XPS and TEM. The corrosion rate of the Ni-base alloys were evaluated through the chemical descale process.

2. Experimental

Ni-Cr-Fe alloys were melted in a vacuum induction furnace and hot-rolled in a temperature range of 1150~1250℃. The hot-rolled plates were cold-rolled to a thickness of about 1.5 mm with a total area reduction of about 70%. Cold-worked samples were solution annealed at 1060~1100℃ for 1.5~6 min followed by water quenching to obtain the equivalent grain size and then thermally treated at 715℃ for 10 h in a vacuum furnace under about 5×10^{-6} torr. The detail information for the Ni-Cr-Fe alloys with an increase in Cr content was summarized in Table 1.

Table 1. Composition, annealing temperature and grain size of Ni-Cr-Fe alloys with an increase in Cr content.

Content (wt%)			*Meal anneal temp. (℃)*	*Grain size (μm)*
Cr	**Fe**	**Ni**		
16	9	bal.	1060	27.7 ± 2.88
19	9	bal.	1070	28.7 ± 5.02
22	9	bal.	1080	26.7 ± 3.26
25	9	bal.	1090	27.7 ± 3.07
30	9	bal.	1100	28.7 ± 3.18

Oxidation test specimens were machined into 15 mm×45 mm×1.5 mm from the each alloy plate for evaluating corrosion rate and smaller pieces were also cut into 5 mm×5 mm×1.5 mm for analyzing surface oxides. All specimens were finished by grinding with SiC paper of #1200 grit and ultrasonically cleaned in acetone, methanol, ethanol, and deionized (DI) water.

The oxidation tests were performed in a 4L autoclave connected to a circulation loop as shown in Fig. 1. A test solution simulating the primary water of PWRs was prepared by dissolving 2 ppm Li and 1,200 ppm B in DI water and its pH was measured as 6.3 at 25℃. The dissolved hydrogen and oxygen concentrations in the solution were controlled to be 35 $cm^3STP/kg{\cdot}H_2O$, lower than 5 ppb, respectively. The oxidation test was conducted for 1,500h in an autoclave maintained at 330℃ under 150 bars.

Corrosion rate of the Ni-Cr-Fe alloys was evaluated by using gravimetric measurement based on a two-step alkaline permanganate (AP) and ammonium citrate (AC) process. The first step was conducted in an aqueous solution containing 1% $KMnO_4$ and 5% NaOH at 90℃ for 30 min, followed by wiping with a cloth and rinsing in DI water. The second step was performed in a 5% ammonium citrate solution at 90 ℃ for 30 min, followed by wiping with a cloth and rinsing in DI water. After both steps, the weights of the specimens were measured using a five-place balance with an accuracy of 10 μg. In this way, the two-step descaling process was repeated on each specimen at least ten times. To correct the base

metal losses from corrosion during the descaling process, the incremental weight losses were reversely linear-extrapolated, according to the ASTM G1-03. Two corrosion specimens with an area of about 15 cm^2 were used to evaluate the corrosion rate of each alloy specimen.

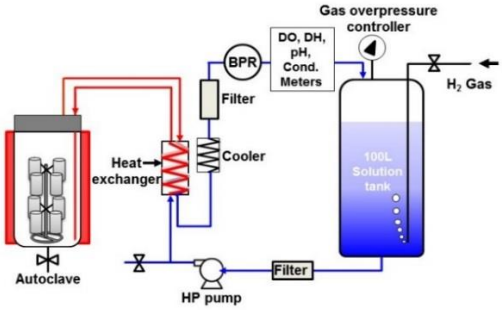

Fig. 1 Schematic of the primary water recirculating system used for the corrosion tests.

The microstructure of the Ni-Cr-Fe alloys were observed using SEM. The specimens were etched in a 2% bromine-98% methanol solution to reveal the microstructure. The average grain size was determined through the intercept procedure specified in the ASTM standard. Structural characteristic of the Ni-Cr-Fe alloys with increasing Cr content was investigated using XRD. The electrochemical properties for the alloys containing Cr contents of 16, 22 and 30 wt% were investigated using a potentiostat and a three-electrode cell in simulated primary solution at 90ºC. An SCE and platinum wire were used as reference and counter electrodes, respectively. The scan rate was 1 mV/s.

The morphology and chemical composition of the oxides formed on the Ni-Cr-Fe alloys with an increase in Cr content were analyzed using SEM and XPS. The microstructure and crystallographic properties of the oxide films on the Ni-Cr-Fe alloys were measured using TEM equipped with EDS and XRD.

3. Results and discussion

The grain size of the Ni-Cr-Fe alloys was equivalently controlled to exclude its effect on oxidation behavior. All specimens were observed to have equiaxed grains of average sizes of 26.7-28.7 ㎛, which are corresponded with an ASTM number of 7.3-7.5 as summarized in Table 1.

Fig. 3 shows the structural characteristics of the Ni-Cr-Fe alloys obtained using XRD. Two characteristic peaks, (111) and (200), were gradually shifted to a lower 2θ value with increasing Cr content. The most intense diffraction peak, (111), is gradually decreased from 44.12° to 43.84° and second intense peak, (200), is also gradually decreased from 51.31° to 51.04° with increasing Cr content. This indicates that the lattice is expanded with the addition of Cr content due to the gradual inclusion of the lager "guest" Cr atoms into the lattice of the smaller "host" Ni atoms. Furthermore, a gradual change in characteristic peaks means that the Cr species are alloyed homogeneously into the Ni matrix.

The anodic polarization curve recorded under potentiodynamic condition for three Ni-Cr-Fe alloys shows an anodic peaks at near 0.6 V followed by a transition to passivity as shown in Fig. 3. Although the corrosion potential value didn't display significant difference, it slightly increased to the negative value as the Cr content in the alloy increased. The passive potentials for three alloys were appeared in similar range of -0.4 V to 0.35 V but the passive current density decreased as the Cr content increased.

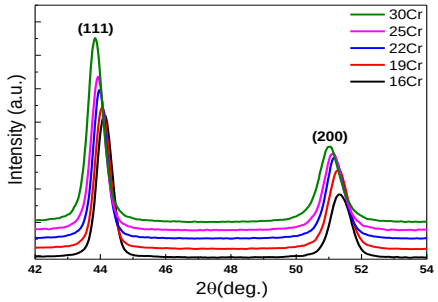

Fig. 2 XRD patterns of Ni-Cr-Fe alloys with increasing Cr content.

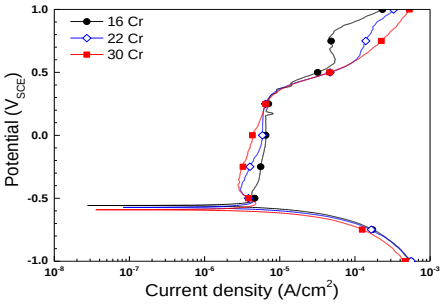

Fig. 3 Potentiodynamic curves of Ni-Cr-Fe alloys including Cr content of 16, 22, and 30 wt% in simulated primary water at 90℃.

Fig. 4 shows the SEM micrographs for the oxidized surfaces of the Ni-Cr-Fe alloys with increasing Cr content. The oxide morphologies of the Ni-Cr-Fe alloys presented a clear difference with increasing Cr content. The wire- and strip-like oxides were mainly observed on the alloys including 16wt%, 19wt%, and 22wt% Cr, whereas the polyhedral oxides were dominantly found on the alloys containing 25wt% and 30wt% Cr. The density of wire- and strip-like oxides was gradually decreased with increasing Cr content and some polyhedral oxides were also observed at some region of the 22wt%-Cr alloy as shown in Fig. 4(c). Some wire-like oxides having a length of tens to hundreds nanometers were only observed on the 25wt%-Cr alloy as shown in Fig. 4(d) and no longer found on the 30wt%-Cr alloy as shown in Fig. 4(e). In addition, it is believed from these results that the wire- and strip-like oxides, which are mainly observed on the alloys having relatively low Cr content, are started to grow as an outer oxide after the polyhedral oxides are formed.

Fig. 5 shows XRD patterns of the oxide films formed on the Ni-Cr-Fe alloys with increasing Cr content. The crystalline peaks of the oxide film of the alloy containing 16wt% Cr were measured at 33.9 ° and 35.7 °, which are corresponded with the characteristic peaks of $NiCrO_3$ and $Ni_{0.4}Fe_{2.6}O_4$, respectively. However, the characteristic peak intensity of $NiCrO_3$ becomes weaker and that of $Ni_{0.4}Fe_{2.6}O_4$ stronger with increasing Cr content,

implying that the crystallinity is enhanced. No characteristic peak of $NiCrO_3$ was observed in the oxide film of the alloys containing Cr content more than 22wt%. This indicates that the Ni-Cr rich oxides is dominantly formed on the alloys having low Cr content but Ni-Fe rich oxides is mainly grown on the alloys having high Cr content.

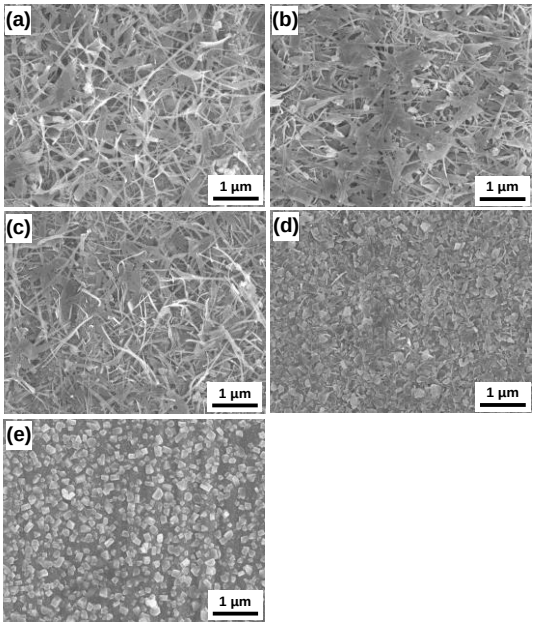

Fig. 4 SEM micrographs of oxide scales formed on Ni-Cr-Fe alloys with increasing Cr content: (a) 16wt%, (b) 19wt%, (c) 22wt%, (d) 25wt%, and (e) 30wt%.

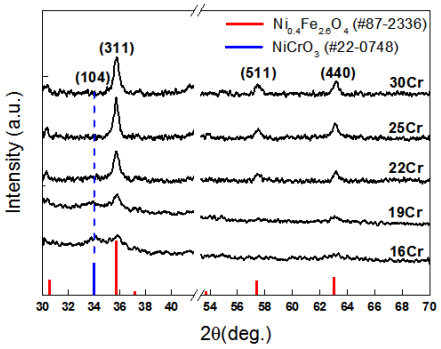

Fig. 5 XRD patterns of the oxide films of Ni-Cr-Fe alloys with increasing Cr content after oxidation test.

To further analyze the effect of the Cr content increase on the oxidation behavior of the Ni-Cr-Fe alloys, STEM image, EDS line profile, and elemental mapping images were obtained for the cross-section of the oxidation specimens of the alloys containing 16wt% and 30wt% Cr, which showed distinct characteristics in the oxide morphology, as shown in Fig. 6 and 7. The cross-sectional morphologies of these oxide films indicated that both of the oxide films consisted of double-layer structure. The oxide film grown on the alloy containing 16wt% Cr was composed of inner oxide layer penetrating randomly into the matrix and outer oxide layer consisting of wires and polyhedral particles as shown in Fig. 6(a). The wire-like oxide was a Ni-rich oxide including small amount of Cr and inner oxide layer displayed by dark-grey color was a Cr-rich oxide as shown in Fig. 6(b). In addition, the Cr depletion region was found around Cr-rich oxide as marked with pink circles and the Ni concentration became high in this region. Fig. 6(c) and 6(d) show the elemental mapping images for the three major alloying elements and oxygen, respectively. The most outer oxide of wire-shape should be mainly nickel oxide and grown from the surface of inner oxide layer. In addition, some polyhedral particles, which were decorated with the wire-like oxides, were Fe-rich oxide including small amount of Ni and Cr. The Cr-rich oxides were randomly networked and deeply penetrated into a metal matrix, resulting some Cr-depleted metallic islands.

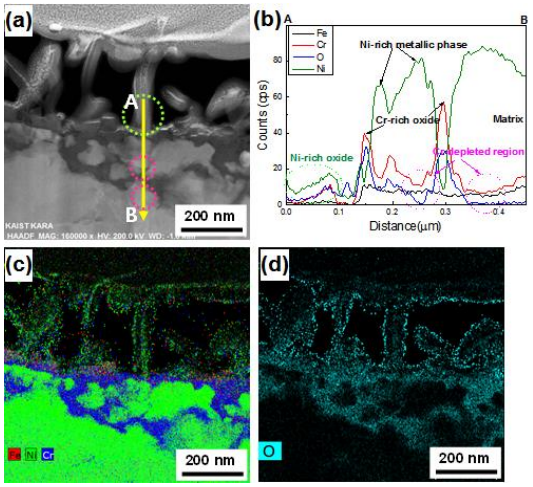

Fig. 6 Cross-sectional (a) STEM image, (b) EDS line profile, (c) and (d) elemental mapping images of the oxide formed on the alloy containing 16wt% Cr.

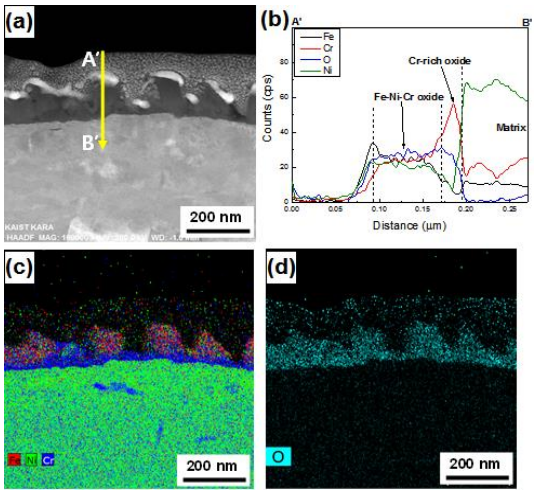

Fig. 7 Cross-sectional (a) STEM image, (b) EDS line profile, (c) and (d) elemental mapping images of the oxide formed on the alloy containing 30wt% Cr.

Whereas, the oxide film of the alloy containing 30wt% Cr was composed of polyhedral particles having the size smaller than 200 nm as an outer oxide and continuous thin layer as an inner oxide as shown Fig. 7. Then, the outer oxide was a Fe-Ni-Cr oxide on the Cr_2O_3 passivation layer having the thickness of 40~50 nm as shown in the EDS profile on A'B' line. The Cr-depletion region was also found in matrix near the Cr-rich oxide layer in the oxide film of the alloy containing 30wt% Cr in Fig. 7(b). This is well corresponded with the results of the elemental mapping data for the major alloying elements and oxygen as shown in Fig. 7(c) and 7(d). The

outer oxide particles was a Fe-Ni-Cr spinel oxide and the Cr_2O_3 thin layer was covered entire surface of metal matrix below these particles. The random penetration of inner oxide layer was not found in the oxide film of the alloy containing 30wt% Cr. However, it was unusual result that some line-shape metallic Cr-rich phases were found in the matrix.

Fig. 8 shows the general corrosion rates of the Ni-base alloys with increasing Cr content. The corrosion rate of the alloy containing 16wt% Cr revealed the highest value of 0.96 mg/m^{2}h and it gradually decrease with increasing Cr content. In addition, the corrosion rate showed the lowest value of 0.11 mg/m^{2}h for the alloy containing 30wt% Cr. Thus, the corrosion rate was lowered by about 88% with increasing Cr content from 16 to 30 wt%. However, no difference was found in corrosion rate for the Ni-Cr-Fe alloys with the Cr content more than 22 wt%.

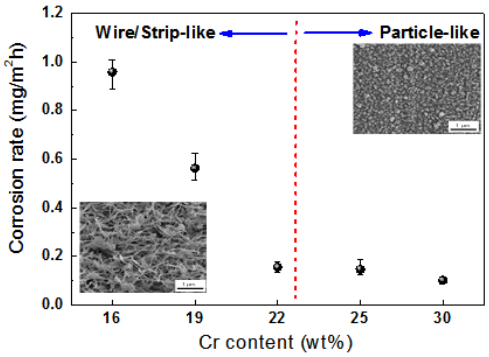

Fig. 8 Corrosion rate of the Ni-Cr-Fe alloys with increasing Cr content.

The results obtained in this work can be summarized as follows: by increasing the Cr content in Ni-Cr-Fe alloy, the XRD characteristic patterns were gradually shifted to lower 2θ, and the corrosion potential increased to negative value and the passive current density decreased. In addition, surface oxide morphology was changed from the wire- and strip-like oxides to polyhedral particle oxides with increase of Cr content, resulting the reduction of corrosion rate. According to Terachi et al. [8], the specimens having higher Cr content is easy to form the passivation layer of chromium oxide phase and it suppress the diffusion of other cations such as Fe^{2+} or Fe^{3+}. Consequentially, the increase of Cr content in alloy leads the reduction of oxide film thickness and change in oxide type.

The effect of Cr content on the oxidation behavior can be discussed from the following viewpoints: diffusion of cation in alloy and passivation layer formation. The addition of Cr content into Ni matrix leads the lattice expansion and the distortion in structure because the size of the guest atom, Cr, is larger than that of the host atom, Ni. Thus, diffusion rate of metallic atoms through alloying structure, which is defined by self-diffusion rate, is declined by addition of larger atom because the activation energy for the diffusion of metal atom increases as the large guest atom is added into the host matrix [9]. Those are well seen in the cross-sectional images of the oxides grown on the Ni-base alloys with different Cr content in Fig. 6 and 7. The passivation layer in the oxides of 16wt%-Cr alloy was not only formed non-homogeneously at original surface and also penetrated irregularly into the matrix. Whereas, the passivation layer in the oxides of 30wt%-Cr alloy was formed as a homogeneous thin layer. This means that the high Cr content in Ni-Cr-Fe alloys facilitates the formation of robust passivation layer. Consequently, this causes that the 30wt%-Cr alloy has superior passivity compared with the 16wt%-Cr alloy. Therefore, it can be understood that the oxide thickness and corrosion rate is greatly reduced by increase of Cr content.

4. Conclusions

We investigated the effect of Cr content increase in the Ni-Cr-Fe alloys on corrosion rate and its oxide formation characteristics in PWR primary water. The corrosion rate was reduced by about 88% with the increase of Cr content from 16 wt% to 30 wt%. The Ni-rich wire-like and strip-like oxides were dominantly formed and the protectiveness of the Cr_2O_3 passive film was reduced as the Cr content decreased. In addition, the amount of Cr content in the Ni-Cr-Fe alloys showed a threshold value of more than 22wt% for corrosion rate. Therefore, the use of the Ni-Cr-Fe alloy with a high Cr content is more advantageous in terms of general corrosion and release for source term reduction. In addition, in order to improve the resistance of corrosion in PWR primary water, the Cr content included in the Ni-Cr-Fe alloys would be at least larger than 22wt%.

Acknowledgments

This work was supported by the National Research Foundation of Korea (NRF) grant funded by the Korea government (2017M2A8A4015159).

REFERENCES

[1] D. Hussey, Source term Reduction: Impact of Plant Design and Chemistry on PWR Shutdown Releases and Dose Rates, EPRI, Palo Alto, CA, USA, 1013507, 2006.
[2] T. Angeliu, G. Was, The effect of chromium, carbon, and yttrium on the oxidation of nickel base alloys in high temperature water, J. Electrochem. Soc. Vol.14, p1877, 1993.
[3] F. Delabrouille, Characterization of cracks of SCC of Ni-base alloys using MET: Effect of chromium content and environment chemistry, INP Toulouse, France, 2004.
[4] R. Staehle, Corrosion Basics in Primary and Secondary Systems of LWRs, Advance Test Reactor National Scientific User Facility, User Week, Idaho Falls, ID, 2009.
[5] P. M. Scott, Stress Corrosion Cracking in Pressurized Water Reactors-Interpretation, Modeling, and Remedies, Corrosion, Vol. 56, p.771, 2000.
[6] S. Fyfitch, Corrosion and Stress Corrosion Cracking of Ni-Base Alloys, Comprehensive Nuclear Materials Vol. 5, p.69, 2012.
[7] C. Gregorich, Pressurized Water Reactor Shutdown Activity Releases-2014 Summary, EPRI, Palo Alto, Ca, USA, 3002005483, 2015.
[8] T. Terachi, R. Yamada, T. Miyamoto, K. Arioka, K. Fukuya, Corrosion Behavior of Satainless Steels in Simulated Primary Water – Effect of Chromium Content in Alloys and Dissolved Hydrogen, J. Nucl. Sci. Technol. Vol. 45, p.975, 2008.
[9] R. Evans III, J. DeVan, G. Watson, Self-diffusion of Chromium in Nickel-base Alloys, ORNL Report 2982, ORNL, Oak Ridge, 1961.